Colloids and Surfaces B: Biointerfaces 245 (2025) 114337

Contents lists available at ScienceDirect

Colloids and Surfaces B: Biointerfaces

journal homepage: www.elsevier.com/locate/colsurfb

Application of electrospinning and 3D-printing based bilayer composite scaffold in the skull base reconstruction during transnasal surgery

Yiqian Zhu [a,b,1], Xuezhe Liu [c,1], Keyi Zhang [a,b,1], Mohamed EL-Newehy [d], Meera Moydeen Abdulhameed [d], Xiumei Mo [c,*], Lei Cao [e,*], Yongfei Wang [a,b,**]

[a] Department of Neurosurgery, Huashan Hospital, Shanghai Medical College, Fudan University, Shanghai 200040, China
[b] National Center for Neurological Disorders, Huashan Hospital, Shanghai Medical College, Fudan University, Shanghai 200040, China
[c] State Key Laboratory for Modification of Chemical Fibers and Polymer Materials, Shanghai Engineering Research Center of Nano-Biomaterials and Regenerative Medicine, College of Biological Science and Medical Engineering, Donghua University, Shanghai 201620, China
[d] Department of Chemistry, College of Science, King Saud University, P.O. Box 2455, Riyadh 11451, Saudi Arabia
[e] Orthopaedic Traumatology, Trauma Center, Shanghai General Hospital, School of Medicine, Shanghai Jiao Tong University, Shanghai 201620, China

ARTICLE INFO

Keywords:
Electrospinning
3D-printing
Tissue engineering
Skull base reconstruction
Transnasal

ABSTRACT

Skull base defects are a common complication after transsphenoidal endoscopic surgery, and their commonly used autologous tissue repair has limited clinical outcomes. Tissue-engineered scaffolds prepared by advanced techniques of electrostatic spinning and three-dimensional (3D) printing was an effective way to solve this problem. In this study, soft tissue scaffolds consisting of centripetal nanofiber mats and 3D-printed hard tissue scaffolds consisting of porous structures were prepared, respectively. And the two layers were combined to obtain bilayer composite scaffolds. The physicochemical characterization proved that the nanofiber mat prepared by polylactide-polycaprolactone (PLCL) electrospinning had a uniform centripetal nanofiber structure, and the loaded bFGF growth factor could achieve a slow release for 14 days and exert its bioactivity to promote the proliferation of fibroblasts. The porous scaffolds prepared with polycaprolactone (PCL), and hydroxyapatite (HA) 3D printing have a 300 μm macroporous structure with good biocompatibility. In vivo experiments results demonstrated that the bilayer composite scaffold could promote soft tissue repair of the skull base membrane through the centripetal nanofiber structure and slow-release of bFGF factor. It also played the role of promoting the regeneration of the skull base bone tissue. In addition, the centripetal nanofiber structure also had a promotional effect on the regeneration of skull base bone tissue.

1. Introduction

Transnasal endoscopic surgery has become the primary procedure for the removal of skull base tumours, yet it frequently results in significant complications, including cerebrospinal fluid leakage and intracranial infections in patients [1,2]. In clinical practice, the primary method for preventing cerebrospinal fluid leakage is skull base reconstruction using autologous tissues (such as fat, broad fascia, or free mesonasal turbinate mucosal flaps) in the postoperative period [3,4]. Nevertheless, the field still confronts significant challenges, including a scarcity of autologous materials, secondary trauma, a postoperative infection rate of 19–21 % [5,6], and a cerebrospinal fluid leakage incidence of 3–5 % [7–9]. In response to these limitations, the development of artificial skull base reconstruction materials has emerged as a pivotal area of investigation in endoscopic skull base surgery. The ideal skull base reconstruction material should exhibit enhanced biocompatibility, degradability, mechanical durability, and bioactivity [10,11]. However, how to obtain materials that have structural similarity to skull base bone and dura mater is the main technical difficulty at present.

Nanofibers can mimic the structure of natural extracellular matrix and facilitate cell adhesion and migration [12,13]. Many studies have shown that the orientation structure of nanofibers also has a good guiding role for cell migration [14]. Electrospinning, as a common technology for preparing nanofibers, has the advantages of processing a

* Corresponding authors.
** Corresponding author at: Department of Neurosurgery, Huashan Hospital, Shanghai Medical College, Fudan University, Shanghai 200040, China
E-mail addresses: xmm@dhu.edu.cn (X. Mo), caoleiseu@163.com (L. Cao), eamns@hotmail.com (Y. Wang).
[1] Yiqian Zhu, Xuezhe Liu and Keyi Zhang contributed equally to this work.

https://doi.org/10.1016/j.colsurfb.2024.114337
Received 5 August 2024; Received in revised form 12 October 2024; Accepted 22 October 2024
Available online 23 October 2024

variety of polymer materials and low cost. In the previous research, through further improvement of the receiving device, we can obtain a centripetal oriented nanofiber mat, and find that it can promote the centripetal growth of cells, which is of great significance for tissue regeneration and healing [15,16]. Therefore, in this study, it is proposed to use electrospinning technology to prepare oriented centripetal nanofiber mat. The mat will used as the repair material after skull base defect, to provide a suitable microenvironment for cell growth and cell adhesion, and to accelerate the repair and regeneration of soft tissue after skull base trauma. In addition, the electrospinning process enables the preparation of products loaded with growth factors, drugs, etc., and the slow-release function to realize their biological functions [17].

For skull base bone defects, the development of 3D printing technology provides a new method for preparing bone tissue engineering scaffolds. As a rapid prototyping technology, 3D printing technology can process a variety of biomaterials to obtain porous scaffolds via layer by layer [18]. This processing technology has a personalized choice, which can customize the scaffold matching the clinical tissue defect repair [19]. In addition, it allows the adjustment of relevant printing parameters in order to obtain macro- and microstructural designs at an early preparation stage [20,21]. Therefore, this study intends to use 3D printing technology to prepare three-dimensional scaffolds that can promote the repair of skull base bone defects.

In this study, we combine bioengineering technology and materials science, seeking to develop an electrospinning and 3D-printing based bilayer composite scaffold. The nanofiber membrane base layer consists of oriented centripetal nanofiber mat loaded with bFGF growth factors to mimic dura tissue and promote soft tissue repair. The 3D printed top layer consists of 3D printed PCL (polycaprolactone) and HA (hydroxyapatite) to exfoliate cranial bone tissue and promote hard tissue repair. At first, the bilayer composite scaffold was prepared and characterized for its basic morphology, mechanical strength and other physicochemical properties. Then in vitro test was used to evaluate the biocompatibility of bilayer composite scaffold. Finally, in vivo test was used to characterize the ability to promote soft and hard tissue repair, by constructing a rabbit cranial defect repair model for cerebrospinal fluid leakage.

2. Materials and methods

2.1. Preparation and modification of bilayer composite scaffolds

To prepare electrospun fibrous membranes, 1 g polylactide-polycaprolactone (PLCL) was dissolved in 10 mL HFIP stirred on a magnetic mixer overnight to obtain PLCL electrospinning solution. The PLCL electrospinning solution was transferred into a syringe. After fixing the syringe on the pump, the voltage was set to 12 kV and the pump speed was set to 1 mL/h. A steel ring (diameter is 14 mm) was used as collector device, and a conductive iron-wire was placed in the middle of the steel ring to prepare the centripetal radially aligned nanofiber mat. Subsequently, PLCL centripetal radially aligned nanofiber mat was obtained under the above spinning parameters. Then, the prepared nanofiber mat was immersed in 2 mg/mL, pH 8.5 of dopamine solution overnight at room temperature to coat a polydopamine film on the surface of the membrane. Then it was subsequently immersed in phosphate buffer solution (PBS) containing 1666 μg/mL bFGF factor to coat the growth factor.

To prepare 3D printed scaffold, 1 g PCL (molecular weight is 80,000) and 0.15 g HA particles (diameter is 20–30 nm) were dissolved in tetrahydrofuran, followed by being stirred on a magnetic mixer for 5 days. HA-PCL composites were obtained after complete evaporation of tetrahydrofuran. For the 3D printing process, the previously obtained PCL/HA composite was cut into small pieces and put into FDM-based 3D printer with a melt temperature of 90°C. After 3D printing, a PCL/HA composite scaffold with a height of 1 mm and an area of 10 mm * 10 mm was obtained. To prepare pure PCL scaffold, 1.15 g PCL were weighed and the rest of the procedures were performed as above.

The process of preparing a bilayer composite scaffold by the underlying nanofiber mats scaffold and the upper bony scaffold was as follows: 1) Contact one side of the 3D printed scaffold with 100°C high-temperature water for 3 s, 2) Press one side of PLCL centripetal radially aligned nanofiber mat on the softened side of 3D printed scaffold. 3) Obtain a bilayer composite scaffold with complete curing after freeze-drying.

2.2. Performance evaluation of bilayer composite scaffold

The surface morphology of the nanofiber mat and 3D printed scaffold were observed by scanning electron microscopy (SEM) of Phenom after 45 s of spraying gold under vacuum condition.

For mechanical testing of the nanofiber mat sample, the oriented nanofiber mat was cut to a long rectangle of 15 mm in length and 5 mm in width, and the thickness was measured. The ends of the rectangle were fixed with a clamp and the stretching rate was set to 1 mm/min. The stress-strain curve of the samples was obtained (n=6).

The nanofiber mats were placed in 24-well, sterilized by UV lamp for 60 min, and 70 % ethanol immersion for 30 min. After the sterilization, 1 mL NIH-3T3 cell suspension (1×10^4/mL) was seed on each well of the cell culture plate, followed by rapid transfer to constant-temperature incubator for culturing. After culturing for 1, 4, and 7 days, the culture plate was washed three times with PBS. Then CCK-8 was added to each well with mats and incubated for 90 min without light. 100 μl from each well was transferred to a 96-well plate, and the absorbance value of each well was measured at 450 nm.

To evaluate the MSC proliferation behavior on 3D printed scaffold, The MSC of rat were isolated by the whole bone marrow adherent method. Use and care of the animals used in this study followed the guidelines established by the Animal Care and Use Committee of the School of medicine of Fudan University. The intact femur and tibia were obtained from healthy male SD rats (Shanghai Jiesijie Laboratory Animal Co., Ltd). After the ends of the tibia and femoral backbone were cut, the bone marrow was flushed using a syringe with fresh medium and then a homogeneous cell suspension was made. The cell suspensions were centrifuged, re-suspended with α-MEM complete medium, and incubated in a 37 ℃ cell culture incubator. When the adherent cells reached 90 % or more, they were recorded as primary cells (P0). Cells at passage 3 were used for the subsequent experiments. After rat MSCs were co-cultured with the 3D printed scaffold, the medium was aspirated from the well plate that were subsequently washed 3 times with PBS. Then 300 μL non-complete medium containing 10 % CCK-8 was added to each well with the scaffold and incubated for 90 min without light. Then 100 μL from each well was transferred to a 96-well plate, and the absorbance value of each well was measured at 450 nm.

To investigate the bFGF release behavior from the nanofiber mat, the samples were sterilized and immersed in 1 mL PBS. After1, 3, 7 and 14 days of release, the sample was removed, and the residual liquid was centrifuged to collect the supernatant. The concentration of bFGF factor in the supernatant was tested according to the instructions of the bFGF ELISA kit.

2.3. Establishment of cerebrospinal fluid leakage model in experimental animals with convex defects of the brain

All experiments were performed on adult male New Zealand big-ear rabbits, aged 3 months and weighing between 2 and 2.5 kg. General anesthesia was administered by intramuscular injection of 0.2 mL/kg of Sumianxin *II* injection. The procedure was strictly aseptic, and a heating blanket was used to maintain the body temperature of the experimental rabbits at 38.5–39.5 °C.

The skull was exposed, and a 15 mm * 15 mm square bone window was opened in the right parietal region using a grinding drilling. Then a 10 mm * 10 mm dural window was opened with microscissors to

confirm the flow of cerebrospinal fluid. After that, a 10 mm*10 mm bilayer composite scaffold was implanted. to cover the window. Tight hemostasis was achieved with interrupted sutures for subcutaneous and skin in layers. The incision was covered with gauze and cephalosporin antibiotic 5 mg/kg was injected intramuscularly. Postoperatively, their behavioral activities, consciousness and vital signs were monitored closely, and the repair for cerebrospinal fluid leakage and other complications such as intracranial infection was observed.

The experimental groups were as follows: control group A (Random nanofiber mat+ PCL/HA scaffold, Random-PCL/HA), experimental group B (centripetal radially aligned nanofiber mat + PCL/HA scaffold, Radially-PCL/HA), experimental group C (bFGF-loaded centripetal radially aligned nanofiber mat + PCL/HA scaffold, Radially/bFGF-PCL/HA), each group of samples was five. The effect of the bilayer composite scaffold in reconstruction repair of dura and skull was evaluated at two time points (1 month, 3 months).

2.4. Evaluation of the effectiveness of bilayer composite scaffold for repair of cranial defects and dural defects

The experimental animals were sacrificed at 1 month and 3 months after surgery. Their skull and dural tissue around the center of the bilayer composite scaffold were removed by grinding drill and fixed with 10 % formalin, and then embedded to make paraffin sections. The sections were fixed with 2.5 % glutaraldehyde, 2 % paraformaldehyde in 0.1 M Sodium Cacodylate (pH 7.2), and post-fixed with 1 % osmium tetroxide solution. The fixed samples were trimmed, dehydrated stepwise in increasing concentrations of acetone and embedded. H&E and Masson staining were performed to detect the proliferation and differentiation and in-growth status of fibroblasts and osteoblasts on the bilayer composite scaffolds of different experimental groups in the in vivo experiments. Apart from above, BrdU staining can examine the ratio of proliferating cells and thus evaluate whether the bilayer composite scaffold bound by bFGF promotes the proliferation of fibroblasts and whether it has a directed growth effect on the migration and coverage of fibroblasts.

Micro-CT scans (Quantum GX2 micro-CT Imaging System, PerkinElmer Inc.) were performed on the skulls, and the images were analyzed quantitatively with CTAn analysis software to evaluate parameters such as new bone volume BV (mm^3), bone surface area density BS/ TV (1/mm) and others.

2.5. Statistical analysis

The mean ± standard error was calculated to describe each group of data. IBM SPSS 23.0 software was used for statistical analysis and GraphPad Prism and Origin for plot description; Analysis of variance was used to infer whether there was a significant difference between the groups ($P < 0.05$, number of groups $\geqq 3$). Holm t-test was used to analyze the differences between groups, while students *t*-test was used to verify the differences between the two data groups. Log-transformed t-test was used to verify whether there was a significant difference in the experimental data after standardizing the corresponding control group.

3. Results

3.1. Preparation and modification of bilayer composite scaffold

Three types of underlying nanofiber mats were prepared by using electrospinning technology: random nanofiber mat scaffold, centripetal radially aligned nanofiber mat scaffold, and bFGF-loaded centripetal radially aligned nanofiber mat scaffold, respectively. Using 3D printing technology, two types of upper scaffolds were prepared respectively: PCL scaffold, and PCL/HA scaffold. Three different combinations of bilayer composite scaffolds were prepared by curing the bottom layer and the top layer together: random nanofiber mat + PCL/HA composite scaffold, centripetal radially aligned nanofiber mat + PCL/HA composite scaffold, and bFGF-loaded centripetal radially aligned nanofiber mat + PCL/HA composite scaffold. The preparation process of the bilayer composite scaffold was shown in Schematic 1.

3.2. Characterization of electrospun nanofiber mat

The radially nanofiber mats were fabricated at first, by using digital camera and SEM to observe the centripetal radially aligned nanofiber mat, it could be seen that the nanofibers in the central structure of the mat were regularly arranged and dense, with uniform dispersion from the center to the periphery (Fig. 1 A, B). Tensile mechanical testing was performed on the centripetal radially aligned nanofiber mat scaffold, while the random nanofiber mat scaffold was prepared as control. The tensile mechanical curves of the lower centripetal oriented membranous scaffold showed that the nanofiber mats had high tensile strength and good ductility (Fig. 1 C, D). The deformation was less than 5 % when external force was higher than 2.0 MPa. Which means that the nanofiber mats can withstand external forces of about 2.0 MPa and has good ductility with a maximum deformation rate of 45 %. Furthermore, compared to random nanofiber mats, radially nanofiber mats have similar Ultimate stress, but higher elongation and low Young's modulus (Fig. 1E).

Using a SEM to observe the cell morphology of fibroblasts grown on the random and radially nanofiber mats, it showed that the centripetal radially nanofiber mat scaffold had a significant guiding effect on the growth of fibroblasts. It also showed more cells adhering to the surface of the radially nanofiber mat compared to random nanofiber mat (Fig. 2). The microscopic morphology of the surface centripetally oriented nanofiber mat can effectively guide cell morphology and proliferation.

Next, the radially nanofiber mat were loaded with bFGF growth factor to prepare Radially/bFGF nanofiber mat. At first, the drug release behavior of bFGF from Radially/bFGF nanofiber mat was investigated by *in vitro* test. It was indicated that the nanofiber mat can gradually and steadily release the bFGF *in vitro*, with an average cumulative release rate of 67.0 % at 14 days (Fig. 3 A). Then, the fibroblasts were seeded on the surface of Radially/bFGF nanofiber mat, while the TCP, Random, and Radially nanofiber mat without bFGF were set as control. The CCK-8 assay results showed that nanofiber mat scaffolds could promote proliferation of fibroblasts *in vitro*, and the nanofiber mat scaffold that loaded with bFGF promoting proliferation of fibroblasts significantly better than that without bFGF (1.75 ± 0.08 vs. 1.03 ± 0.14, $p < 0.001$) (Fig. 3B).

3.3. Characterization of 3D printed scaffold

In order to prepare the bone tissue scaffold for skull base bone regeneration, PCL/HA was used to print an 3D printed scaffold. Digital camera and SEM images showed that the 3D printed scaffold were fabricated with porous structures, and the pore size was 300 μm approximately (Fig. 3 C). The proliferation of MSC of 3D printed scaffold was performed by CCK-8 assay. MSCs showed better proliferation behavior on the 3D printed scaffolds compare to TCP control *in vitro,* but with no significant difference seen between group PCL and group PCL/HA (0.66 ± 0.34 vs. 0.59 ± 0.30, $p = 0.719$) (Fig. 3D).

3.4. Evaluation of the effectiveness of bilayer composite scaffold for the repair of cranial and dural defects

A cranial defect model was applied to investigate the cerebrospinal fluid leakage repairment. 1*1 cm^2 bone and dural window was removed to release cerebrospinal fluid and expose brain tissue. A bilayer composite scaffold (top layer was electrospun nanofiber mat, bottom layer was 3D printed scaffold) was placed under direct vision at the site of the skull and dural defects (Fig. 4A-C). After 1 and 3 months postoperative,

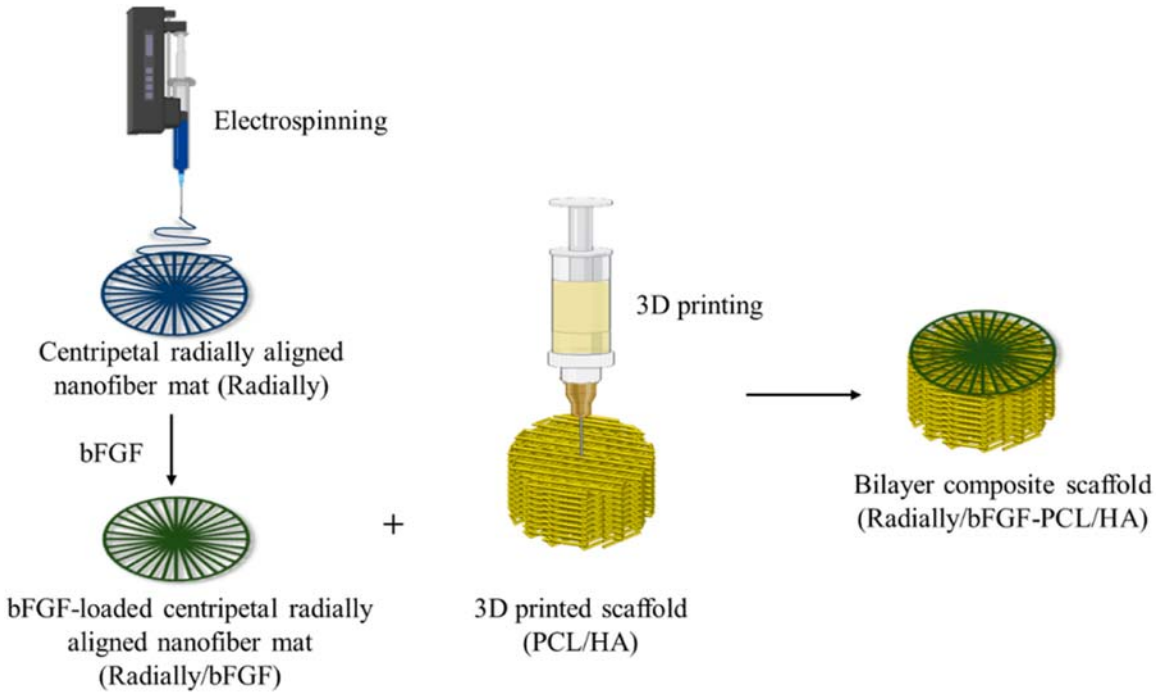

Schematic 1. The preparation process of bilayer composite scaffold.

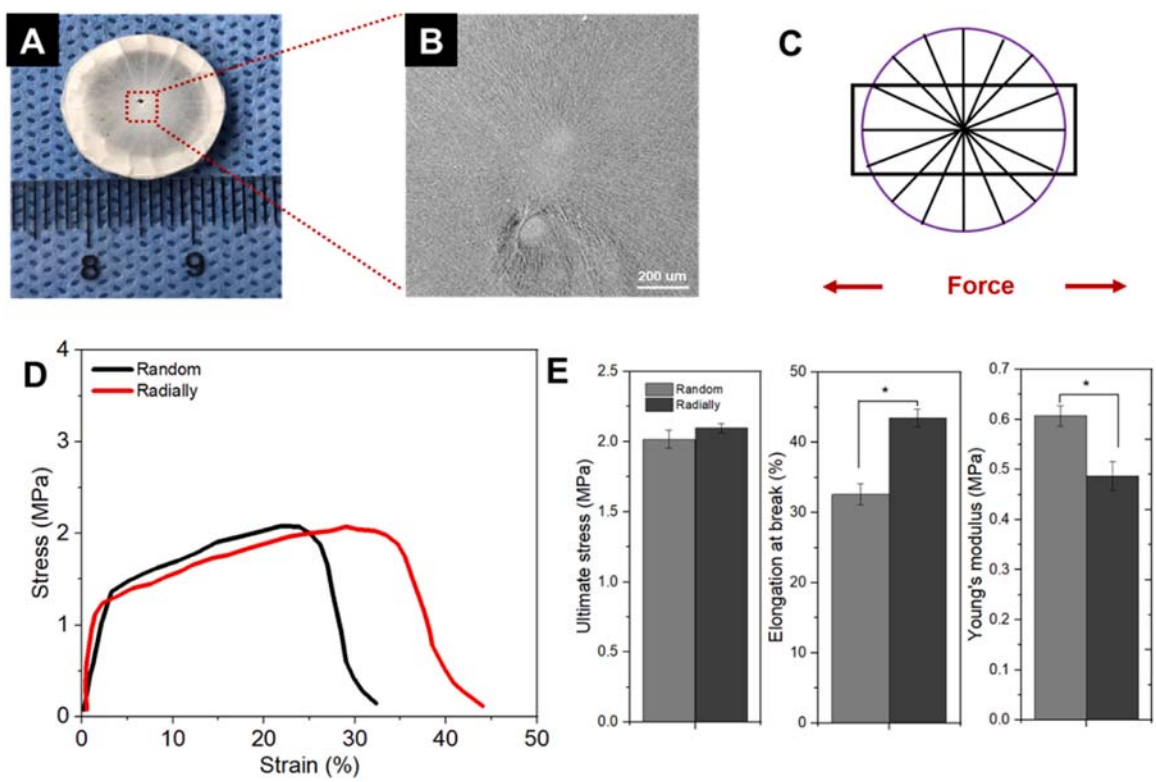

Fig. 1. (A) Physical picture and (B) SEM image of the centripetal radially aligned nanofiber mat with a diameter of about 1 cm. (C) Tensile mechanics testing for centripetal radially aligned nanofiber mat. (D) Strain-stress curve of random and radially nanofiber mats. E. Ultimate stress, elongation at breaks and Young's modulus of random and radially nanofiber mats.

the animals were sacrificed for further characterization (Fig. 4D, E). H&E staining sections at 1 month postoperatively showed that the bilayer composite scaffold at the site of the skull and dural defect was tightly connected to the surrounding tissue, a small amount of inflammatory cell infiltration was seen in all groups of different scaffolds. The bilayer composite scaffold in group Random-PCL/HA was well connected to the surrounding tissue structure, and inflammatory cells and foreign body giant cells were present around the scaffold, with a small amount of new fibrous connective tissue and bone tissue hyperplasia. In groups Radially-PCL/HA and Radially/bFGF-PCL/HA, new bone tissue

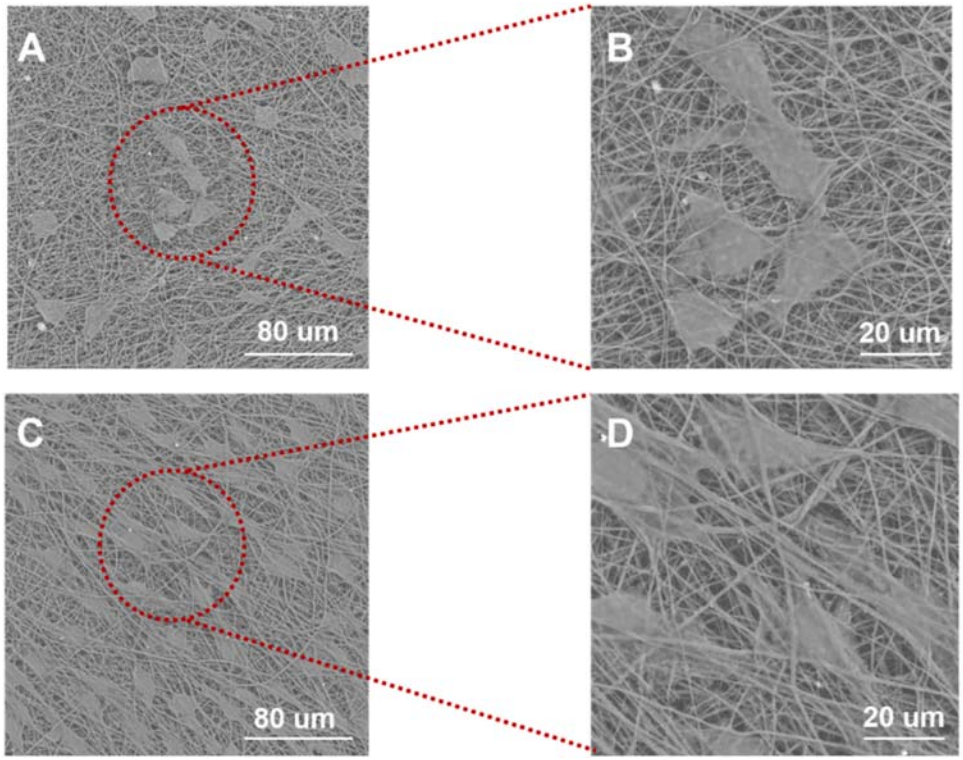

Fig. 2. SEM images of fibroblasts cell morphology on (A, B) random nanofiber mat and (C, D) radially nanofiber mat.

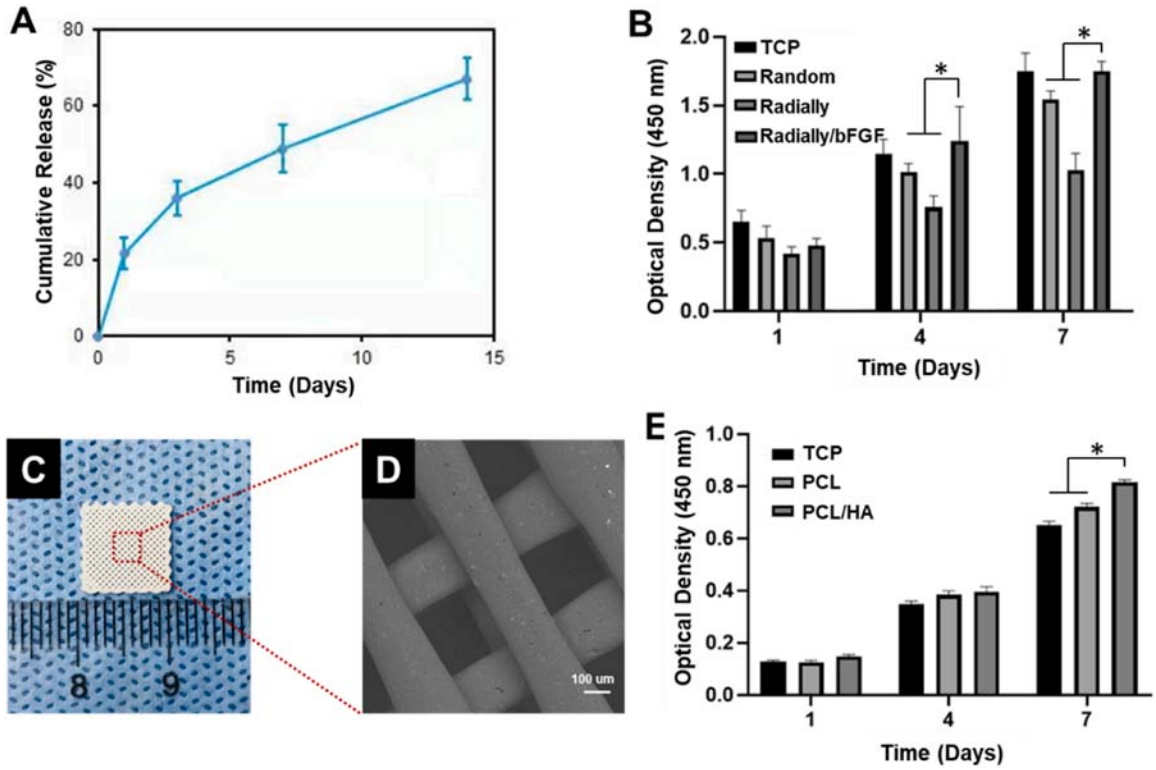

Fig. 3. (A) bFGF release curves of the bFGF loaded radially nanofiber mat in vitro experiment. (B) CCK-8 assay of fibroblasts on TCP, Random, Radially, and Radially/bFGF nanofiber mats. (C) Physical picture and (D) SEM image of the 3D printed PCL/HA scaffold. (E) CCK-8 assay of MSC cells on TCP, PCL and PCL/HA scaffolds.

grew inside the porous scaffold and interconnected channels supported the guide of bone regeneration. More fibrous connective tissue and bone matrix proliferation increased in group Radially/bFGF-PCL/HA compared to other groups. while largest amount of matured dense bone tissue appears in group Radially/bFGF-PCL/HA. (Fig. 4F). These results reveal that porous interconnected structure and HA can

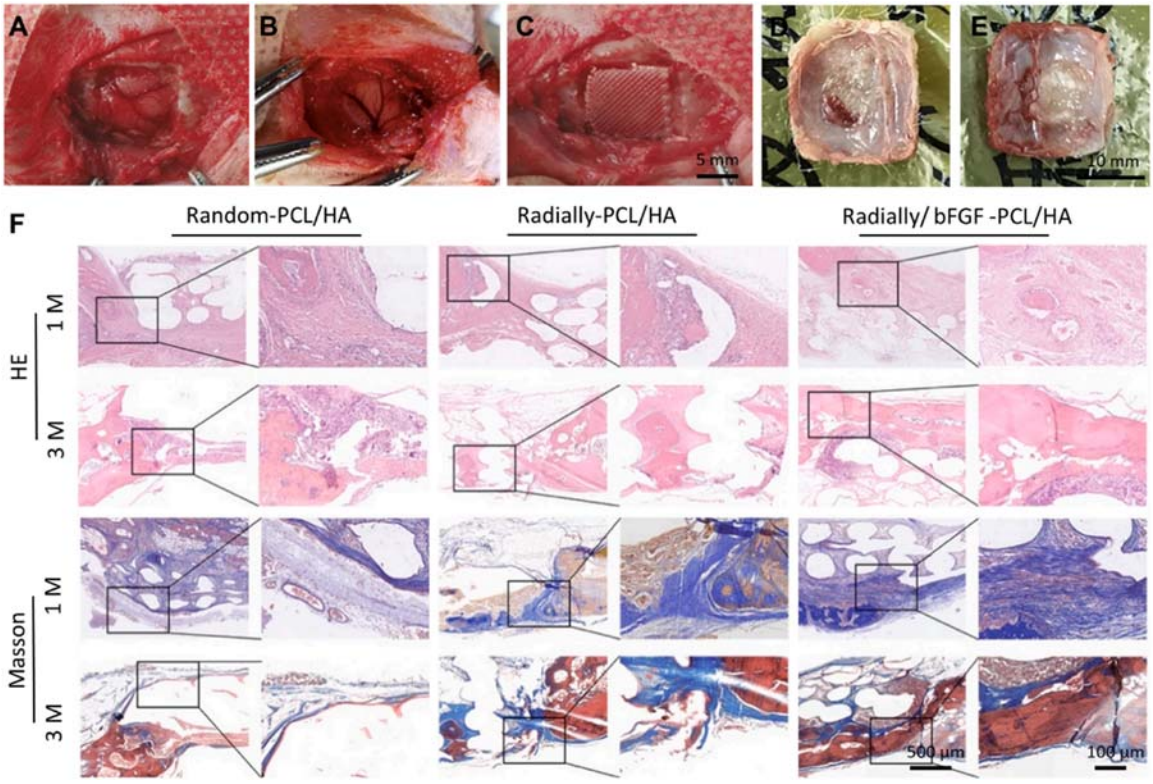

Fig. 4. Bilayer composite scaffolds regenerate dura mater and bone tissue in vivo. (A) The bone window was opened and the dural layer was exposed. (B) The dural window was opened to expose the brain tissue. (C) The bilayer composite scaffold was placed at the site of the skull and dural defect. Anatomical drawings of the location of the bilayer composite scaffold at (D) 1 month and (E) 3 months postoperatively, including the surrounding skull and dural tissue. (F) HE and Masson histologic staining results of three bilayer composite scaffolds at 1 and 3 months after surgery.

efficiently stimulate bone regeneration.

H&E and Masson staining at 3 months postoperatively showed that the scaffolds in different experimental groups were well integrated with the surrounding tissues. H&E staining showed the amount of new fibrous tissue and bone tissue was significantly increased compared to all groups at 3 months, and the new connective tissue was growing continuously along the scaffold orientation. Masson staining revealed significantly red staining of mature collagen in PCL/HA groups at 3 months, while many immature collagens of blue staining are observed in PCL/HA groups at 1 month. The largest area of mature collage appears in group3 at 3 months, which shows a prominent osteogenic ability. Furthermore, mature collagen tissue grew continuously along the scaffold with a tight structure (Fig. 4F).

In order to investigate the radially nanofiber structure and bFGF effect for tissue regeneration. Brdu staining at the defect site of the bilayer composite scaffold implanted at 3 months after surgery. It was showed that the number of Brdu-stained cells in the Radially/bFGF-PCL/HA group was significantly higher than that in other two groups, suggesting more active cell proliferation (Fig. 5 A).

Micro-CT scan images of the skull of experimental rabbits at 3 months postoperatively, and it was used for analysis the bone regeneration with quantitative (Fig. 5B). Quantitative analysis of new bone volume BV (mm^3) and bone surface area density BS/TV (1/mm) showed that the PCL/HA group loaded with bFGF was significantly better than Random-PCL/HA group, and the differences of means in BV (37.66 ± 14.73 vs. 12.06 ± 2.75, P = 0.005) and BS/TV (4.92 ± 0.16 vs. 4.53 ± 0.10, P = 0.002) were statistically significant. There were no significant differences in BV (36.66 ± 14.73 vs 33.83 ± 14.43, P = 0.674) and BS/TV (4.92 ± 0.16 vs 4.88 ± 0.14, P = 0.692) between PCL/HA groups with or without bFGF (Fig. 5 C).

4. Discussion

Nasal leakage of cerebrospinal fluid is one of the most common and serious complications of endoscopic transnasal surgery that disrupts the normal bony and membranous structures at the base of the skull, leading to intracranial communication with the outside world. Intraoperative reconstruction and repair of the skull base defect is the key to prevent cerebrospinal fluid leakage and intracranial infection [22]. Autologous soft tissues such as fat and expanded fascia are commonly used for skull base membrane reconstruction, but there is a lack of corresponding bone tissue regeneration materials. In this study, we innovatively propose the use of synthetic materials PLCL, PCL, HA, and bFGF factors, combined with advanced centripetal orientation electrospinning and 3D printing technologies, to simultaneously prepare bilayer integrated soft and hard tissue scaffolds for simultaneous repair and regeneration of both cranial basement membrane soft tissues and cranial hard tissues.

For soft tissue regeneration, we first propose to use centripetal electrostatic spinning technique to prepare nanofiber mats with centripetal structure. Electrospinning can prepare nanofibrous materials that mimic the structure of extracellular matrix, which was widely used for human dural repair [23,24]. In this study, we propose to prepare nanofibers with centripetal structure, which can better guide the migration and growth of cells centripetally relative to nanofibers with random structure, as we can prove by SEM results of cell proliferation. In addition, this oriented structure allows this nanofiber mat to have a higher Young's modulus, which might be due to that the oriented structure can improve its mechanical properties [25]. The loading of bFGF onto nanofiber mats is another key technology for the preparation of biologically active tissue engineering scaffolds [26,27]. In this study, bFGF was modified on the surface of the nanofiber mat by using chemical grafting, and a sustained release of 67.0 % for 2 weeks was obtained. This slow-release capacity could sustain the bioactivity of the

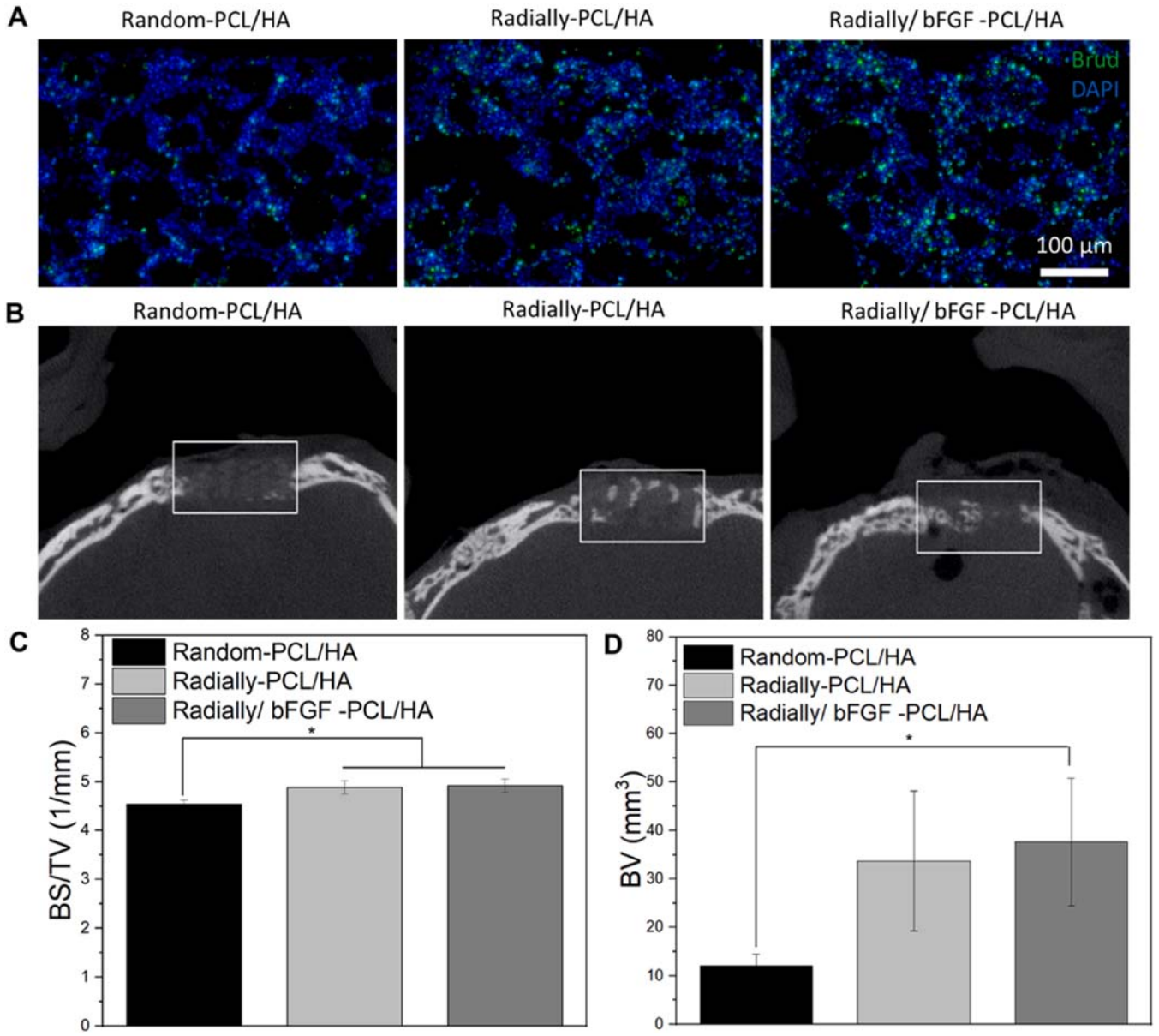

Fig. 5. (A) Brdu staining of implanted bilayer composite scaffolds was showed in the Random-PCL/HA, Radially-PCL/HA, and Radially/bFGF-PCL/HA groups, respectively. (B) Micro-CT scan images of the skull defect reveal different bone continuity in three groups at 3 months postoperatively. (C) Quantitative analysis of new bone volume BV (mm^3), and bone surface area density BS/TV (1/mm) in three groups at 3 months postoperatively.

growth factor, and it was demonstrated that the slow-released bFGF showed better promotion of fibroblast proliferation in vitro by CCK-8 assay. Further by constructing animal experiments, after the comparison of Random-PCL/HA, Radially-PCL/HA and Radially/bFGF-PCL/HA in three groups at 1 month and 3 months postoperatively, H&E and Masson staining showed that the scaffolds in each group were well integrated with the surrounding tissues, which indicated that the bilayer composite scaffolds had a good biocompatibility. However, connective tissue and collagen fiber deposition around the nanofibrous mat with centripetal structure and slow-release bFGF was more than the other two groups, suggesting that it was more conducive to soft-tissue repair, as evidenced by Brdu fluorescence staining results. The previous studies have shown that bFGF can effectively shorten the time of wound healing in the process of wound healing and can promote the proliferation of cells in the local area, the activation of phagocyte aggregation and the formation of neovascularization and improve the perfusion of blood flow [28]. Rat meningeal-derived fibroblasts can express bFGF in the process of in vitro cultivation and can form abundant capillary beds in the transplanted area, which promotes the damaged tissues' regeneration [29]. In addition, it has been shown that this nanofiber structure also prevents cerebrospinal fluid leakage [30,31]. Therefore, the present study demonstrated that the slow release of bFGF factors from the bilayer composite scaffolds may promote rapid soft tissue repair.

For hard tissue repair, we proposed the use of 3D printed PCL and HA composites. The successful preparation of 3D printed scaffolds can be seen from the SEM results. The scaffolds have a higher number of square pore structures of about 300 μm inside the scaffolds, which is of great significance for the tissue repair [32,33]. CCK-8 results are also the results which show that the scaffolds have a good cellular compatibility, and the addition of HA had a promoting effect on the proliferation of MSC cells [34]. In view of the large number of studies in which both materials, PCL and HA, have been used in composite preparation of bone tissue engineering scaffolds, no specific materialistic and cytological studies were performed in this study on the addition or non-addition of hydroxyapatite. Through in vivo experiments, we can see that all three bilayer composite scaffolds achieved pro-cranial hard tissue repair and

regeneration to some extent. It should be noted that MIcro-CT 3D reconstruction and result analysis showed no significant difference in osteogenic regeneration between Radiall-PCL/HA and Radially/bFGF-PCL/HA groups, indicating that nanofiber mat-loaded bFGF was only useful for soft tissue regeneration, but did not show significant promotion for hard tissue regeneration. However, the new bone volume and bone density of both groups were significantly higher than those of the Random-PCL/HA group, suggesting that the centripetally oriented nanofiber mats have a certain promotional effect on bone regeneration, which is complex and may be synchronized with the promotion of soft tissue repair. There is no specific study on this, which is a limitation of this study, and we will further explore the specific role of centripetally oriented structure for hard tissue repair on future studies.

In summary, we developed bilayer scaffolds in this study. The lower layer is a nanofibrous membrane with a centripetal radial pattern, loaded with bFGF growth factor to enhance rapid repair and regeneration of dural tissues after skull base defects. The upper layer is PCL containing hydroxyapatite, created via 3D printing, intended to aid in cranial tissue repair after such defects. Safety was confirmed through in vitro experiments, and effectiveness was validated in vivo, highlighting its potential application value.

5. Conclusion

In order to promote the reconstruction of soft and hard tissues in skull base defects, a bilayer composite scaffold was successfully prepared in this study by electrospinning and 3D printing. SEM results showed that the soft tissue portion had a centripetally oriented nanofibrous structure, and that this structure not only guided the directional growth of fibroblasts, but also improved its mechanical properties. The hard tissue part consists of a regular macroporous structure with a size of 300 μm, which also showed good biocompatibility. The constructed bilayer composite scaffolds were subjected to experiments in the rabbit skull base defect model, and as a result, the oriented nanofibrous structure of the surface soft tissue portion and the loaded bFGF greatly promoted soft tissue repair, while its oriented nanofibrous structure was also shown to promote hard tissue repair. In conclusion, this study demonstrates the potential application of bilayer composite scaffolds for promoting the repair of skull base defects.

CRediT authorship contribution statement

Yongfei Wang: Writing – review & editing, Visualization, Funding acquisition, Conceptualization. **Lei Cao:** Writing – review & editing, Visualization, Data curation, Conceptualization. **Xiumei Mo:** Writing – review & editing, Visualization, Methodology, Funding acquisition. **Meera Moydeen Abdulhameed:** Writing – review & editing, Conceptualization. **Mohamed EL Newehy:** Writing – review & editing, Methodology, Conceptualization. **Keyi Zhang:** Writing – original draft, Methodology, Data curation. **Xuezhe Liu:** Methodology, Investigation, Data curation. **Yiqian Zhu:** Writing – original draft, Project administration, Methodology, Investigation, Data curation.

Declaration of Competing Interest

The authors declare that they have no known competing financial interests or personal relationships that could have appeared to influence the work reported in this paper.

Acknowledgements

This project was supported by Science and Technology Commission of Shanghai Municipality, China (20DZ2254900). This project was also supported by Researchers Supporting Project Number (RSPD2024R769), King Saud University, Riyadh, Saudi Arabia.

Data availability

No data was used for the research described in the article.

References

[1] H.M. Hegazy, R.L. Carrau, C.H. Snyderman, A. Kassam, J. Zweig, Transnasal endoscopic repair of cerebrospinal fluid rhinorrhea: a meta-analysis, Laryngoscope 110 (2000) 1166–1172.
[2] H.W. Tsai, W.C. Chao, Y.H. Lee, Y.T. Tsai, M.S. Tsai, Y.C. Lee, Sublabial excision versus transnasal endoscopic marsupialization for nasolabial cysts: A systematic review and meta-analysis, Clin. Otolaryngol. 49 (2024) 102–108.
[3] S. Shibao, K. Yoshida, R. Sasao, M. Nishimoto, Prevention of Cerebrospinal Fluid Leakage in the Anterior Transpetrosal Approach, J. Clin. Med. 13 (2024) 1718.
[4] S. Wang, S. Ren, J. Wang, M. Chen, H. Wang, C. Chen, Dural reconstruction materials for the repairing of spinal neoplastic cerebrospinal fluid leaks, ACS Biomater. Sci. Eng. 9 (2023) 6610–6622.
[5] H. Ozawa, M. Sekimizu, S. Saito, S. Nakamura, T. Mikoshiba, Y. Watanabe, Y. Ikari, M. Toda, K. Ogawa, Risk factor for cerebrospinal fluid leak after endoscopic endonasal skull base surgery: a single-center experience, Acta Otolaryngol. 141 (2021) 621–625.
[6] V.E. Staartjes, C.M. Zattra, K. Akeret, N. Maldaner, G. Muscas, C.H.B. van Niftrik, J. Fierstra, L. Regli, C. Serra, Neural network–based identification of patients at high risk for intraoperative cerebrospinal fluid leaks in endoscopic pituitary surgery, J. Neurosurg. 133 (2019) 329–335.
[7] R.J. Harvey, P. Parmar, R. Sacks, A.M. Zanation, Endoscopic skull base reconstruction of large dural defects: a systematic review of published evidence, Laryngoscope 122 (2012) 452–459.
[8] S.J. Johans, D.J. Burkett, K.N. Swong, C.R. Patel, A.V. Germanwala, Antibiotic prophylaxis and infection prevention for endoscopic endonasal skull base surgery: our protocol, results, and review of the literature, J. Clin. Neurosci. 47 (2018) 249–253.
[9] B.D. Thorp, S.B. Sreenath, C.S. Ebert, A.M. Zanation, Endoscopic skull base reconstruction: a review and clinical case series of 152 vascularized flaps used for surgical skull base defects in the setting of intraoperative cerebrospinal fluid leak, Neurosurg. Focus 37 (2014). E4.
[10] C.E. Bailey, C.H. Le, Allografts and Materials in Skull Base Reconstruction, Skull Base Reconstr.: Manag. Cereb. Fluid Leaks Skull Base Defects (2023) 119–147.
[11] U. Spetzger, V. Vougioukas, J. Schipper, Materials and techniques for osseous skull reconstruction, Minim. Invasive Ther. Allied Technol. 19 (2010) 110–121.
[12] X. Zhang, L. Li, J. Ouyang, L. Zhang, J. Xue, H. Zhang, W. Tao, Electroactive electrospun nanofibers for tissue engineering, Nano Today 39 (2021) 101196.
[13] X. Xie, Y. Chen, X. Wang, X. Xu, Y. Shen, A. Aldalbahi, A.E. Fetz, G.L. Bowlin, M. El-Newehy, X. Mo, Electrospinning nanofiber scaffolds for soft and hard tissue regeneration, J. Mater. Sci. Technol. 59 (2020) 243–261.
[14] J. Xue, T. Wu, J. Qiu, S. Rutledge, M.L. Tanes, Y. Xia, Promoting cell migration and neurite extension along uniaxially aligned nanofibers with biomacromolecular particles in a density gradient, Adv. Funct. Mater. 30 (2020) 2002031.
[15] J. Xue, T. Wu, J. Qiu, Y. Xia, Accelerating cell migration along radially aligned nanofibers through the addition of electrosprayed nanoparticles in a radial density gradient, Part. Part. Syst. Charact. 39 (2022) 2100280.
[16] Q. Wang, S. Zhang, J. Jiang, S. Chen, S. Ramakrishna, W. Zhao, F. Yang, S. Wu, Electrospun radially oriented berberine-PHBV nanofiber dressing patches for accelerating diabetic wound healing, Regen. Biomater. (2024) rbae063.
[17] Z. Hussain, H.E. Thu, S.-F. Ng, S. Khan, H. Katas, Nanoencapsulation, an efficient and promising approach to maximize wound healing efficacy of curcumin: A review of new trends and state-of-the-art, Colloids Surf. B. Biointerfaces 150 (2017) 223–241.
[18] M. Mirkhalaf, Y. Men, R. Wang, Y. No, H. Zreiqat, Personalized 3D printed bone scaffolds: A review, Acta Biomater. 156 (2023) 110–124.
[19] C. Wang, W. Huang, Y. Zhou, L. He, Z. He, Z. Chen, X. He, S. Tian, J. Liao, B. Lu, 3D printing of bone tissue engineering scaffolds, Bioact. Mater. 5 (2020) 82–91.
[20] Z. Geng, W. She, W. Zuo, K. Lyu, H. Pan, Y. Zhang, C. Miao, Layer-interface properties in 3D printed concrete: Dual hierarchical structure and micromechanical characterization, Cem. Concr. Res. 138 (2020) 106220.
[21] H. Gonabadi, Y. Chen, A. Yadav, S. Bull, Investigation of the effect of raster angle, build orientation, and infill density on the elastic response of 3D printed parts using finite element microstructural modeling and homogenization techniques, Int. J. Adv. Manuf. Technol. (2022) 1–26.
[22] R.J. Schlosser, W.E. Bolger, Nasal cerebrospinal fluid leaks: critical review and surgical considerations, Laryngoscope 114 (2004) 255–265.
[23] B. Campbell, Z. Anderson, D. Han, I. Nebor, J. Forbes, A.J. Steckl, Electrospinning of cyanoacrylate tissue adhesives for human dural repair in endonasal surgery, J. Biomed. Mater. Res. Part B: Appl. Biomater. 110 (2022) 660–667.
[24] J. Xie, M.R. MacEwan, W.Z. Ray, W. Liu, D.Y. Siewe, Y. Xia, Radially aligned, electrospun nanofibers as dural substitutes for wound closure and tissue regeneration applications, ACS nano 4 (2010) 5027–5036.
[25] S.-d Liu, D.-s Li, Y. Yang, L. Jiang, Fabrication, mechanical properties and failure mechanism of random and aligned nanofiber membrane with different parameters, Nanotechnol. Rev. 8 (2019) 218–226.
[26] X. Yu, P. Yue, X. Peng, H. Ding, N. Lei, X. Yu, A dural substitute based on oxidized quaternized guar gum/porcine peritoneal acellular matrix with improved stability, antibacterial and anti-adhesive properties, Chin. Chem. Lett. 34 (2023) 107591.

[27] S. Sahoo, L.T. Ang, J.C.H. Goh, S.L. Toh, Growth factor delivery through electrospun nanofibers in scaffolds for tissue engineering applications, J. Biomed. Mater. Res. Part A: Off. J. Soc. Biomater., Jpn. Soc. Biomater., Aust. Soc. Biomater. Korean Soc. Biomater. 93 (2010) 1539–1550.
[28] S. Akita, K. Akino, A. Yakabe, K. Tanaka, K. Anraku, H. Yano, A. Hirano, Basic fibroblast growth factor is beneficial for postoperative color uniformity in split-thickness skin grafting, Wound Repair Regen. 18 (2010) 560–566.
[29] S. Chrissouli, H. Pratsinis, V. Velissariou, A. Anastasiou, D. Kletsas, Human amniotic fluid stimulates the proliferation of human fetal and adult skin fibroblasts: the roles of bFGF and PDGF and of the ERK and Akt signaling pathways, Wound Repair Regen. 18 (2010) 643–654.
[30] S. Sun, H. Luo, Y. Wang, Y. Xi, K. Fang, T. Wu, Artificial spinal dura mater made of gelatin microfibers and bioadhesive for preventing cerebrospinal fluid leakage, ChCom 60 (2024) 2353–2356.
[31] Y. Wang, Q. Guo, W. Wang, Y. Wang, K. Fang, Q. Wan, H. Li, T. Wu, Potential use of bioactive nanofibrous dural substitutes with controlled release of IGF-1 for neuroprotection after traumatic brain injury, Nanoscale 14 (2022) 18217–18230.
[32] N. Abbasi, S. Hamlet, R.M. Love, N.-T. Nguyen, Porous scaffolds for bone regeneration, J. Sci.: Adv. Mater. Devices 5 (2020) 1–9.
[33] G. Hannink, J.J.C. Arts, Bioresorbability, porosity and mechanical strength of bone substitutes: what is optimal for bone regeneration? Injury 42 (2011) S22–S25.
[34] V.S. Kattimani, S. Kondaka, K.P. Lingamaneni, Hydroxyapatite—Past, present, and future in bone regeneration, Bone Tissue Regen. Insights 7 (2016). BTRI-S36138.